

Effectively Non-oscillatory Regularized L_1 Finite Elements for Particle Transport Simulations

Weixiong Zheng^{a,*}, Ryan G. McClarren^a

^a*Nuclear Engineering, Texas A&M University, College Station, TX 77843-3133*

Abstract

In this work, we present a novel regularized L_1 (RL_1) finite element spatial discretization scheme for radiation transport problems. We review the recently developed least-squares finite element method in nuclear applications and then derive an L_1 finite element by minimizing the L_1 norm of the transport residual. To ensure stability, we develop a consistent L_1 boundary condition (BC). Our method requires a nonlinear solve that we treat as a series of weighted least-squares calculations. The numerical tests demonstrate that our method removes the numerical artifacts that arise in LS solutions in problems with voids and pure absorbers. In these problems, our method gives non-oscillatory solutions. We also show that only a few iterations of the nonlinear solver give significant improvement over the standard LS solution.

Keywords: L_1 norm; minimization; least-squares finite element method; non-oscillatory; radiation transport

1. Introduction

Neutral particle transport problems are governed by the linear Boltzmann transport equation, a first-order, hyperbolic equation for the phase space density of particles. The streaming operator in the transport equation is a linear advection operator. Consequently, problems where particles travel long distances

*Corresponding author
Email addresses: zwxne2010@gmail.com (Weixiong Zheng), rgm@tamu.edu (Ryan G. McClarren)

between scattering interactions, so-called streaming-dominated problems, e.g. void and strong absorber problems, can have discontinuous solutions, a fact that spatial discretization schemes should respect. On the other hand, in regions where particles travel very short distances between scattering interactions, the transport equation asymptotically limits to a diffusion equation. There has been much research into methods that are asymptotic preserving for this limit [1, 2]. At present the most widely used spatial discretization scheme that can handle both discontinuous solutions in the streaming dominated case and preserves the asymptotic diffusion limit is the discontinuous finite element method (DFEM)[3, 4]. DFEM is widely used despite the notorious disadvantage of requiring additional degrees of freedom compared with the continuous finite element method (CFEM) that is commonly used in elliptic and parabolic problems.

Another approach to solve transport problems recasts the transport equation into a symmetric, second-order form. This can be done by deriving even-parity equations and self-adjoint angular flux equations[5, 6, 7, 8, 9] or by using the least-squares finite element method. The least-squares finite element method seeks solutions in a finite element space to minimize the squared residual of the transport equation. The minimizer of the squared residual is the solution to the weak form of a symmetrized transport equation. Thereafter, CFEM can be used to solve this transport equation. Recent work has successfully applied least-squares finite elements to a variety of transport applications[10, 11, 12, 13, 14, 15, 16, 17, 18].

There remain a number of open problems regarding least-squares finite elements. For instance, using an under-resolved mesh in problems with strong absorbers can induce oscillations and negative particle densities[19, 20, 21, 22]. These negative densities, in addition to being non-physical, yield nonsensical reaction rates, which are usually the primary quantity of interest for particle transport simulations. Moreover, in multi-D situations, void or near-void situations can also induce negativity in the particle density due to oscillations caused by the existence of discontinuities in the solution to the continuum equations. These oscillations exist even in solutions to the first-order transport with

DFEM[22] when piecewise linear or high-degree basis functions are used. Even without oscillations, void regions can induce low accuracy of the least-squares method without specific corrections [12]. Yet, in real-world problems, like radiation shielding problems or remote sensing, those situations are usual and inevitable.

For the least-squares (LS) method, one cause of the oscillations is that the L_2 norm of transport residual overestimates the contribution from large residual components. Like least-squares fitting in data analysis, when trying to fit every single data point, the fitting principle would overweight the contribution from large-error points, leading to erroneous and oscillatory results[23, 24]. One of the remedies is to develop finite elements that minimize the residual of the transport equation in other norms, such as L_1 . This is difficult because the L_1 norm is non-smooth and typically requires the solution of nonlinear equations. Previously, Jiang developed the iteratively reweighted least-squares (IRLS) method for linear advection[24]. The IRLS method uses a power of the inverse residual as the weighting function for a least-squares method. For simplicity, IRLS uses an approximation to the residual in the weighting function and assumes the weighting function to be constant in each spatial cell. The rationale behind this choice is that such a method would approximate the L_1 norm-induced method. It was shown that for discontinuous boundary data, IRLS is extremely accurate in the interior of the domain. However, Lowrie and Roe [25] demonstrated that IRLS does not necessarily propagate information correctly from boundary so that if the incident boundary condition (BC) is smooth, IRLS can give erroneous results. In particular, large gradients of the solution can be mistakenly treated as discontinuities. Furthermore, Lowrie and Roe demonstrated that IRLS is not an L_1 method.

In a more recent work, by developing efficient nonlinear solving techniques, Guermond approximated the L_1 solution for several problems in fluid dynamics based on Newton's method[26]. The L_1 method is demonstrated to be accurate and stable in problems where least-squares has difficulty and oscillations and accurately treats smooth solutions in contrast to Lowrie's findings about

IRLS. Yet, Guermond’s implementation of L_1 does not have a continuum form, making it difficult to apply to problems of particle transport where strong interactions could dominate advection. It also lacks a theory for consistent boundary conditions, which is required for many transport problems.

We wish to have a method with stability property of the L_1 method, as demonstrated by Guermond, with an implementation that builds on the technology recently developed for least-squares finite elements. Therefore, we introduce a regularized L_1 method for solving particle transport problems. Such a method is designed to be a regularized version of L_1 method in the sense that L_1 method will be used only when the pointwise residual becomes larger than certain criteria otherwise the least-squares method is used. Additionally, the scheme is designed to be compatible with source iteration and acceleration techniques like diffusion synthetic acceleration (DSA)[27] that are de rigeur for efficiently solving transport problem. We also develop a consistent L_1 BC which, as we will demonstrate, is necessary to obtain accurate solutions.

The remainder of this paper is organized as follows: in Sec. 2, we derive the LS weak formulation solving one-speed steady-state radiation transport equation; we then derive an L_1 and further a regularized L_1 (RL_1) finite element method in a continuum form in Sec. 3. Therein, we further derive the consistent L_1 and RL_1 boundary weak formulation to prevent oscillations on incident boundaries. We briefly discuss the details of the implementation. Thereafter, we demonstrate the method efficacy in Sec. 4. We conclude the work in Sec. 5.

2. Least-Squares Method for One-speed Neutron Transport Equation

2.1. One-speed transport equation

Given that we are interested in spatial discretization of the transport equation, we will restrict ourselves in this work to steady state, energy-independent transport problems, with isotropic scattering and volumetric fixed source. Extending our method with time and energy dependence and anisotropic scattering is relatively straightforward using existing methods.

The steady, mono-energetic transport equation is given by [28, 29, 6]:

$$\vec{\Omega} \cdot \nabla \psi(\vec{r}, \vec{\Omega}) + \sigma_t(\vec{r})\psi(\vec{r}, \vec{\Omega}) = \frac{\sigma_s \phi(\vec{r})}{4\pi} + \frac{Q(\vec{r})}{4\pi}, \quad \vec{r} \in \mathcal{D} \quad (1)$$

where $\vec{\Omega} \in \mathbb{S}_2$ is the directional vector on the unit sphere corresponding to the direction of travel for particles; ψ is the angular flux with units of particles per unit area per steradian per second; σ_s and σ_t are respectively the scattering and total cross sections with units of inverse length; ϕ is the scalar flux defined as

$$\phi(\vec{r}) = \int_{4\pi} d\Omega \psi(\vec{r}, \vec{\Omega});$$

Q is the isotropic volumetric fixed source.

The boundary conditions for Eq. (1) specify ψ for incoming directions on the boundary:

$$\psi(\vec{r}, \vec{\Omega}) = \psi^{\text{inc}}(\vec{r}, \vec{\Omega}), \quad \vec{r} \in \partial\mathcal{D}, \quad \vec{\Omega} \cdot \hat{n} < 0,$$

where $\hat{n}(\vec{r})$ is the unit outward normal on the boundary of the domain.

For notational simplicity, we will also use the operator form as the following:

$$\mathcal{L}\psi = q_s, \quad (2)$$

where \mathcal{L} is the streaming plus removal operator

$$\mathcal{L} \equiv \vec{\Omega} \cdot \nabla + \sigma_t,$$

and the total (fixed plus scattering) source is

$$q_s \equiv \frac{\sigma_s \phi(\vec{r})}{4\pi} + \frac{Q(\vec{r})}{4\pi}.$$

We will discretize the angular component of the transport equation using the discrete ordinates (S_N) method [7] where we use a quadrature set for the angular space, $\{w_n, \vec{\Omega}_n\}$, to obtain N equations of the form

$$\mathcal{L}_n \psi_n = q_s,$$

where $\psi_n = \psi(\vec{r}, \vec{\Omega}_n)$,

$$\mathcal{L}_n \equiv \vec{\Omega}_n \cdot \nabla + \sigma_t,$$

and

$$\phi(\vec{r}) \approx \sum_{n=1}^N w_n \psi_n(\vec{r}).$$

On the boundary we write $\psi_n(\vec{r}) = \psi^{\text{inc}}(\vec{r}, \vec{\Omega}_n)$ for $\vec{r} \in \partial\mathcal{D}$ and $\vec{\Omega}_n \cdot \hat{n} < 0$.

This choice of angular discretization will not affect the derivation of our spatial discretization. Therefore, we will drop the n subscripts in the following sections. For example, we could use our regularized L_1 method with the spherical harmonics treatment of the angular variable.

2.2. Interior Weak Form of the Least-Squares Discretization

To derive a LS discretization of the transport equation, we begin with defining the L_2 norm of transport residual $R = \mathcal{L}\psi - q_s$ away from the boundary of the domain:

$$\Gamma_{L_2}(\psi) = \int_{4\pi} d\Omega \int_{\mathcal{D}} d\vec{r} R(\psi)^2, \quad (3)$$

where we have restricted ψ to belong to a finite element space \mathcal{V} .

We next introduce an arbitrarily small perturbation ϵv , where $\epsilon > 0$ is an arbitrarily small number and v is a weight function in the finite element space \mathcal{V} . Then we obtain the perturbed functional:

$$\Gamma_{L_2}(\psi + \epsilon v) = \int_{4\pi} d\Omega \int_{\mathcal{D}} d\vec{r} (R(\psi + \epsilon v))^2. \quad (4)$$

To minimize the functional, we expect the first derivative to be zero in order to find the stationary point in the finite element space [30], i.e.

$$\left. \frac{\partial \Gamma_{L_2}}{\partial \epsilon} \right|_{\epsilon=0} = \int_{4\pi} d\Omega \int_{\mathcal{D}} d\vec{r} \mathcal{L}v (\mathcal{L}\psi - q_s) = 0. \quad (5)$$

Therefore, after rearranging, we have the weak formulation for the interior: find $\psi \in \mathcal{V}$ such that for any $v \in \mathcal{V}$

$$\int_{4\pi} d\Omega \int_{\mathcal{D}} d\vec{r} \mathcal{L}v \mathcal{L}\psi = \int_{4\pi} d\Omega \int_{\mathcal{D}} d\vec{r} \mathcal{L}v q_s. \quad (6)$$

2.3. Boundary condition and complete weak formulation

It is straightforward as well to obtain a weak form for the BC for the LS method. Similar to Eq. (3), we define the functional for the BC measured by the L_2 norm:

$$\Gamma_{b,L_2} = \int_{\vec{n} \cdot \vec{\Omega} < 0} d\Omega \int_{\partial\mathcal{D}} ds \lambda \left| \vec{n} \cdot \vec{\Omega} \right| (\psi - \psi^{\text{inc}})^2, \quad (7)$$

where λ is a cross section related multiplier and defined as:

$$\lambda = \begin{cases} \sigma_t, & \sigma_t > 0, \\ 1.0, & \text{otherwise.} \end{cases} \quad (8)$$

For the non-void situation, the LS weak form is globally conservative[15, 6] with the choice in Eq. (8). The first choice of λ in void is somewhat arbitrary, but has been observed to be adequate. With the same procedure as in Sec. 2.2, we arrive at the boundary weak form:

$$\int_{\vec{n} \cdot \vec{\Omega} < 0} d\Omega \int_{\partial\mathcal{D}} ds \lambda \left| \vec{n} \cdot \vec{\Omega} \right| v\psi = \int_{\vec{n} \cdot \vec{\Omega} < 0} d\Omega \int_{\partial\mathcal{D}} ds \lambda \left| \vec{n} \cdot \vec{\Omega} \right| v\psi^{\text{inc}}. \quad (9)$$

Combining this result with Eq. (6), we reach the complete LS weak form:

$$\begin{aligned} & \int_{4\pi} d\Omega \int_{\mathcal{D}} d\vec{r} \mathcal{L}v\mathcal{L}\psi + \int_{\vec{n} \cdot \vec{\Omega} < 0} d\Omega \int_{\partial\mathcal{D}} ds \lambda \left| \vec{n} \cdot \vec{\Omega} \right| v\psi = \\ & \int_{4\pi} d\Omega \int_{\mathcal{D}} d\vec{r} \mathcal{L}vq_s + \int_{\vec{n} \cdot \vec{\Omega} < 0} d\Omega \int_{\partial\mathcal{D}} ds \lambda \left| \vec{n} \cdot \vec{\Omega} \right| v\psi^{\text{inc}}. \end{aligned} \quad (10)$$

3. Derivation in L_1 Norm

3.1. Smoothed L_1 norm and L_1 finite element method

Similar to the LS method, we begin by defining the L_1 norm of the transport residual:

$$\Gamma_{L_1}(\psi) = \int_{4\pi} d\Omega \int_{\mathcal{D}} d\vec{r} |R(\psi)| \quad (11)$$

A suitable finite element method would be developed by minimizing the functional above. With the procedure introduced in Sec. 2.2, we obtain a perturbed functional:

$$\Gamma_{L_1}(\psi + \epsilon v) = \int_{4\pi} d\Omega \int_{\mathcal{D}} d\vec{r} |R(\psi + \epsilon v)|, \quad v \in \mathcal{V}, \quad \epsilon > 0 \quad (12)$$

However, the functional Γ_{L_1} is not differentiable at the points where $R = 0$. To find the fixed point of Eq. (12) we develop an approximate L_1 norm, as in [20, 19]. For a small number ζ we approximate

$$|R| \approx \sqrt{R^2 + \zeta^2}. \quad (13)$$

Figure 1 illustrates the effect of the approximation for different values of ζ . With decreasing ζ , $\sqrt{x^2 + \zeta^2}$ converges to $|x|$ rapidly.

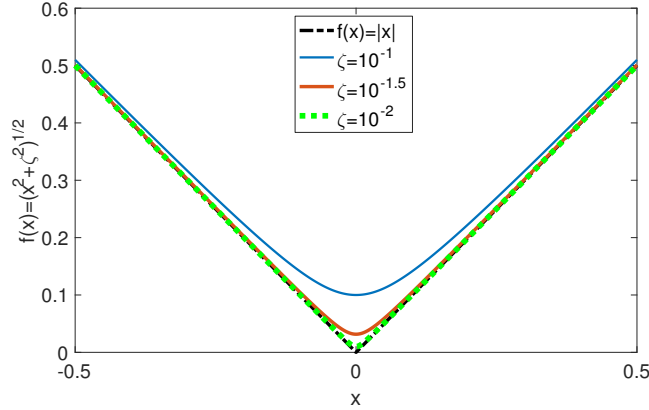


Figure 1: $\sqrt{x^2 + \zeta^2}$ vs $|x|$ for different ζ values.

Introducing Eq. (13) into (12), we obtain a differentiable approximation to the perturbed L_1 norm functional:

$$\Gamma_{L_1}(\psi + \epsilon v) \approx \int_{4\pi} d\Omega \int_{\mathcal{D}} d\vec{r} \sqrt{R(\psi + \epsilon v)^2 + \zeta^2}. \quad (14)$$

To minimize the convex functional, in the finite element space \mathcal{V} , we need to

find its stationary point where the derivative is zero:

$$\frac{\partial \Gamma_{L_1}}{\partial \epsilon} \Big|_{\epsilon=0} = \int_{4\pi} d\Omega \int_{\mathcal{D}} d\vec{r} \frac{\mathcal{L}v(\mathcal{L}\psi - q_s)}{\sqrt{R^2 + \zeta^2}} = 0. \quad (15)$$

Taking the limit $\zeta \rightarrow 0$, the smoothed L_1 expression limits to the L_1 weak form as $\sqrt{R^2 + \zeta^2} \rightarrow |R|$ for $|R| \neq 0$:

$$\int_{4\pi} d\Omega \int_{\mathcal{D}} d\vec{r} \frac{\mathcal{L}v(\mathcal{L}\psi - q_s)}{|R|} = 0, \quad (16)$$

or equivalently,

$$\int_{4\pi} d\Omega \int_{\mathcal{D}} d\vec{r} \frac{\mathcal{L}v\mathcal{L}\psi}{|R|} = \int_{4\pi} d\Omega \int_{\mathcal{D}} d\vec{r} \frac{\mathcal{L}vq_s}{|R|}. \quad (17)$$

This is equivalent to the weak form for the LS finite element with a weighting function that depends on the solution. Clearly, this weak formulation is nonlinear because the evaluation of $|R|$ requires the solution $|\psi|$.

3.2. An L_1 BC

The naïve BC for the L_1 method would use BC from the LS weak form. However, we have observed that the application of this BC causes stability problems on the incident boundaries. A hypothesis is that the norms measuring residuals on the boundary and the interior should be consistent.

We can derive a regularized L_1 BC similar to the approach used for the interior functional. Namely, we write

$$\Gamma_{b,L_1} = \int_{\vec{n} \cdot \vec{\Omega} < 0} d\Omega \int_{\partial\mathcal{D}} ds \lambda \left| \vec{n} \cdot \vec{\Omega} \right| |\psi - \psi^{\text{inc}}|. \quad (18)$$

A boundary weak form as the following can be achieved through similar minimization process as above:

$$\int_{\vec{n} \cdot \vec{\Omega} < 0} d\Omega \int_{\partial\mathcal{D}} ds \lambda \left| \vec{n} \cdot \vec{\Omega} \right| \frac{v\psi}{|\psi - \psi^{\text{inc}}|} = \int_{\vec{n} \cdot \vec{\Omega} < 0} d\Omega \int_{\partial\mathcal{D}} ds \lambda \left| \vec{n} \cdot \vec{\Omega} \right| \frac{v\psi^{\text{inc}}}{|\psi - \psi^{\text{inc}}|}. \quad (19)$$

3.3. L_1 and regularized L_1 weak forms

Whence we have the complete L_1 finite element weak formulations:

$$\begin{aligned} & \int_{4\pi} d\Omega \int_{\mathcal{D}} d\vec{r} \frac{\mathcal{L}v\mathcal{L}\psi}{|R|} + \int_{\vec{n}\cdot\vec{\Omega}<0} d\Omega \int_{\partial\mathcal{D}} ds \lambda \left| \vec{n}\cdot\vec{\Omega} \right| \frac{v\psi}{|\psi - \psi^{\text{inc}}|} \\ &= \int_{4\pi} d\Omega \int_{\mathcal{D}} d\vec{r} \frac{\mathcal{L}vq_s}{|R|} + \int_{\vec{n}\cdot\vec{\Omega}<0} d\Omega \int_{\partial\mathcal{D}} ds \lambda \left| \vec{n}\cdot\vec{\Omega} \right| \frac{v\psi^{\text{inc}}}{|\psi - \psi^{\text{inc}}|} \end{aligned} \quad (20)$$

Due to the assumption of letting ζ vanish, the weak form above is an exact L_1 finite element formulation. However, solving such a weak form can be extremely challenging, especially when residual in the problem varies by several orders of magnitude and when the residual vanishes in certain regions. Instead, we propose a regularized L_1 formulation using a factor $\theta > 0$:

$$\begin{aligned} & \int_{4\pi} d\Omega \int_{\mathcal{D}} d\vec{r} \frac{\theta\mathcal{L}v\mathcal{L}\psi}{\max(\theta, |R|)} + \int_{\vec{n}\cdot\vec{\Omega}<0} d\Omega \int_{\partial\mathcal{D}} ds \lambda \left| \vec{n}\cdot\vec{\Omega} \right| \frac{\theta v\psi}{\max(\theta, |\psi - \psi^{\text{inc}}|)} \\ &= \int_{4\pi} d\Omega \int_{\mathcal{D}} d\vec{r} \frac{\theta\mathcal{L}vq_s}{\max(\theta, |R|)} + \int_{\vec{n}\cdot\vec{\Omega}<0} d\Omega \int_{\partial\mathcal{D}} ds \lambda \left| \vec{n}\cdot\vec{\Omega} \right| \frac{\theta v\psi^{\text{inc}}}{\max(\theta, |\psi - \psi^{\text{inc}}|)}. \end{aligned} \quad (21)$$

This regularization is such that in regions with moderate to large residuals, i.e. $|R| > \theta$, the regularization factor

$$\frac{\theta}{\max(\theta, |R|)} \rightarrow \frac{\theta}{|R|}$$

and the L_1 weak form is used. On the other hand, when the residual is small, the regularization factor goes to 1 and the least-squares weak form is used.

Numerical experiments indicate that the solution is largely insensitive to the choice of θ . The effects of varying it will be illustrated in Sec. 4.1. Normally, we choose θ to be around $0.01|R|_{\text{max}}$, where $|R|_{\text{max}}$ denotes the maximum absolute residual of all direction and space. Smaller θ can be used, yet, we observe the efficiency of the linear solver is degraded without a concomitant gain in solution accuracy.

In our implementation the residuals are evaluated on each spatial quadrature point. This is one of the drawbacks of this method in that it requires storing or performing on-the-fly calculations of the point wise residuals.

3.4. Nonlinear solution method

As RL_1 is nonlinear, an appropriate nonlinear scheme is necessary in order to solve Eq. (21). We will use a Picard iteration scheme that evaluates the residual using the estimate of ψ from the previous iteration. The scheme is initialized using the unweighted least-squares solution. The steps in the solution are

1. Calculate pointwise residuals for Nonlinear Iteration (NI) l from NI $l - 1$;
2. Update the weak form Eq. (21);
3. Solve Eq. (21)
4. Given a nonlinear tolerance tol , check nonlinear convergence $e = \frac{\|\phi^l - \phi^{l-1}\|}{\|\phi^l\|}$:
 - (1) If $e < tol$, stop.
 - (2) else, go to Step 1.

In the solution of Eq.(21) source iteration with diffusion synthetic acceleration (DSA) is utilized[7, 14]. Though RL_1 , as well as LS, does not have consistent low order diffusion acceleration scheme[14], we have found that DSA is still effective. Developing a consistent DSA scheme for LS and RL_1 should be the target of future work.

4. Numerical Results

All numerical results below used finite element solutions carried out with the C++ Open source library `deal.II`[31]. In this section, we present four 2D test problems with bilinear finite elements on rectangular meshes. We first investigate the behavior of RL_1 in void with discontinuous incident BC.

4.1. Void problem

As mentioned above transport problems in voids can contain numerical artifacts such as oscillations and negative solutions due to the discontinuous nature of the analytic solution [21, 19, 20, 22]. A demonstration of these phenomena can be seen in the solution to a beam problem at a grazing angle entering a void from the boundary. The solution to this problem is discontinuous with

solution being zero outside the volume within the view of the beam. Schemes such as LS will have Gibbs oscillations due to the discontinuity. Figure 2 shows the LS and RL_1 solution for this a 2-D void with where the domain is a 0.5×0.5 cm square. Along part of the boundary from $x = 0.1$ to 0.3 cm there is a unit incident angular flux at the angle $\vec{\Omega} = (1/\sqrt{3}, 1/\sqrt{3}, 1/\sqrt{3})$. The unit incident BC is applied only on part of the boundary. The LS solution oscillates near the discontinuity, and has an overshoot of 7%. The RL_1 solution, on the other hand, is monotone and non-negative.

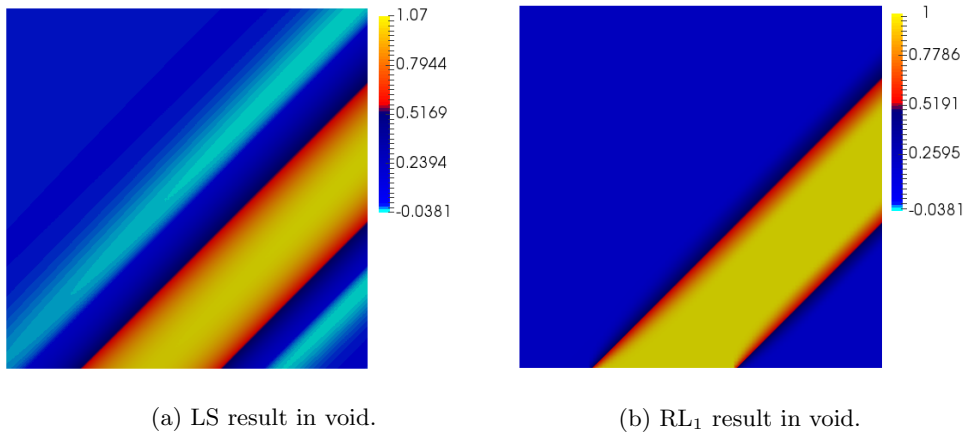


Figure 2: LS and RL_1 method comparison in void transport problem with a grazing, incident flux on the boundary. 100×100 cells are used

This problem can also demonstrate the necessity of having a boundary condition based on L_1 . In Figure 3 we compare the analytic, LS, and RL_1 solutions along the boundary at $y = 0$. In the RL_1 solution we use the L_1 boundary condition we derived above, and the standard LS boundary condition. As seen in the figure, the LS solution does over and under shoot the analytic solution. When the RL_1 method is used with the LS boundary condition, the result is a sharp oscillation near the discontinuity. These oscillations go away when the L_1 -based boundary condition is used.

The results in the previous two figures were performed with $\theta/|R|_{\max} = 0.01$. In Figure 4 we show the line out of the solution $y = 0.2$ cm with differing values

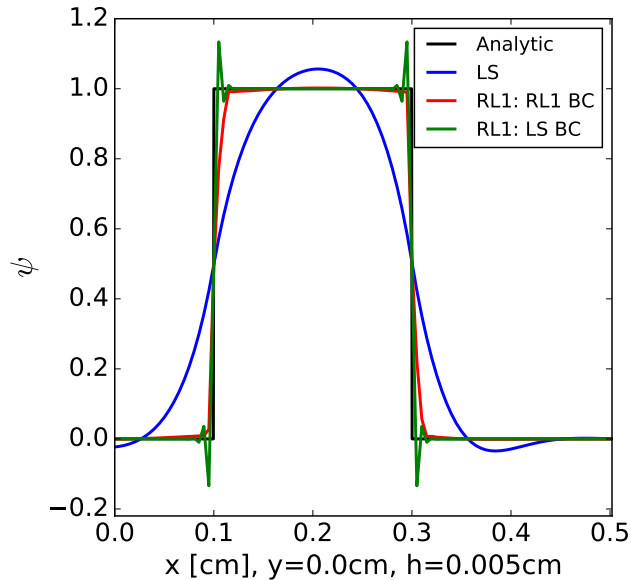


Figure 3: LS and RL_1 with different boundary conditions on the void problem.

of $\theta/|R|_{\max}$. With a large value of θ (the one with $\theta/|R|_{\max} = 0.1$), RL_1 is able to effectively damp the oscillations around the discontinuous solution, though the solution does become slightly negative. The results with $\theta/|R|_{\max} = 0.01$ and 0.0001 are nearly indistinguishable in the figure. For this reason we will use $\theta/|R|_{\max} = 0.01$ for the remainder of this work.

As the mesh is uniformly refined we observe that the errors in the solution to the void problem decrease as the mesh size h to the one-half power for both methods, as illustrated in Figure 5, yet, the constant is smaller for the RL_1 solutions. The converged RL_1 solutions have the smallest error. Typically, a converged solution requires around 40 nonlinear iterations with $tol = 1 \times 10^{-4}$ used in this work. But only a few nonlinear iterations can provide a noticeable improvement over LS.

4.2. Pure absorber problem

The second test is with the same geometry as in the previous problem with the void replaced by an absorber with $\sigma_t = 1.0 \text{ cm}^{-1}$. Additionally, the unit

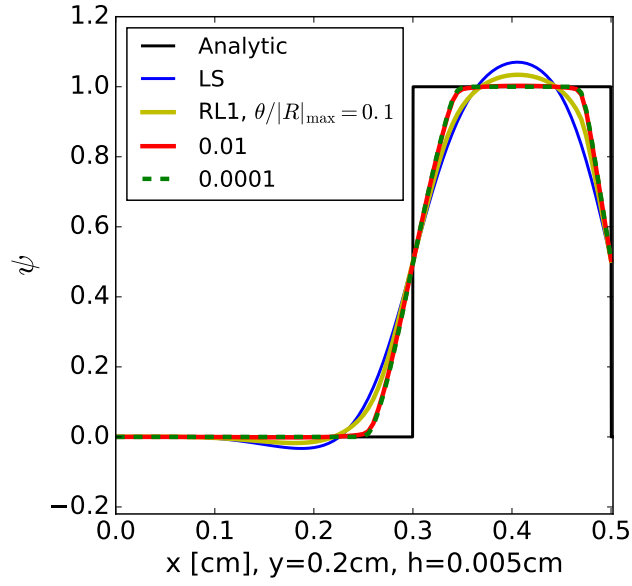


Figure 4: Solution to the void problem at $y = 0.2$ cm for different values of $\theta/|R|_{\max}$.

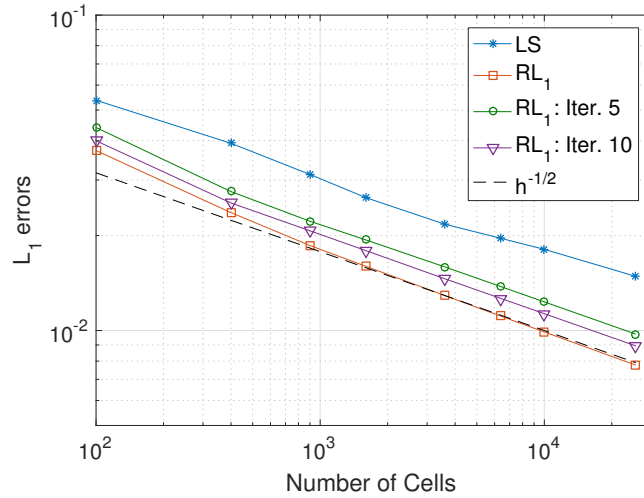


Figure 5: Void problem convergence results.

incident angular flux is imposed through the whole bottom boundary with the same incident angle. Figures 6a and 6b present the angular flux for this problem.

In the pseudo-color plots in Figure 6b we observe the oscillations and negative values in the LS solution; these artifacts do not appear in the RL_1 solution. Figure 7b compares RL_1 and LS line-outs along $y=0.2$ cm with the analytic solution. Indeed, neither of these methods resolves the discontinuity. However, the RL_1 solution is monotonic, in contrast to LS's oscillatory flux as a result of Gibbs phenomenon. We examine the L_1 error of scalar fluxes as well. As the convergence tests in Figure 7a shows, we found both LS and RL_1 have a convergence order near one half, with RL_1 having lower error magnitudes as expected.

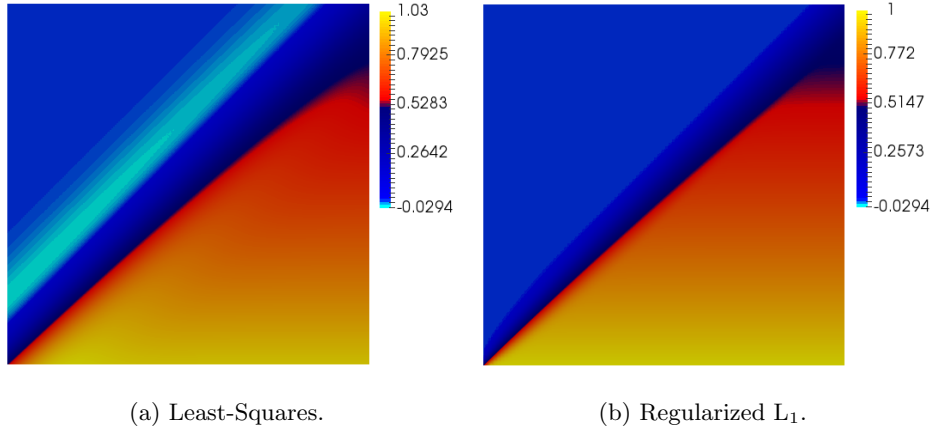


Figure 6: Angular flux distributions in incident convergence test.

4.3. Smooth boundary problem

In this test, we still use the same material and geometry configurations as in Sec. 4.2 except that we use a smooth boundary condition specified at a grazing direction, $\Omega_x = 0.8688$, $\Omega_y = 0.3599$, $\Omega_z = 0.3599$. The boundary condition for this angle is

$$\psi^{\text{inc}} = \begin{cases} \frac{1}{2} + \frac{1}{2} \cos\left(2\pi \frac{x-0.2}{0.2}\right), & x \in (0.1, 0.3) \text{ cm}, y = 0 \text{ cm}, \\ 0, & \text{otherwise.} \end{cases} \quad (22)$$

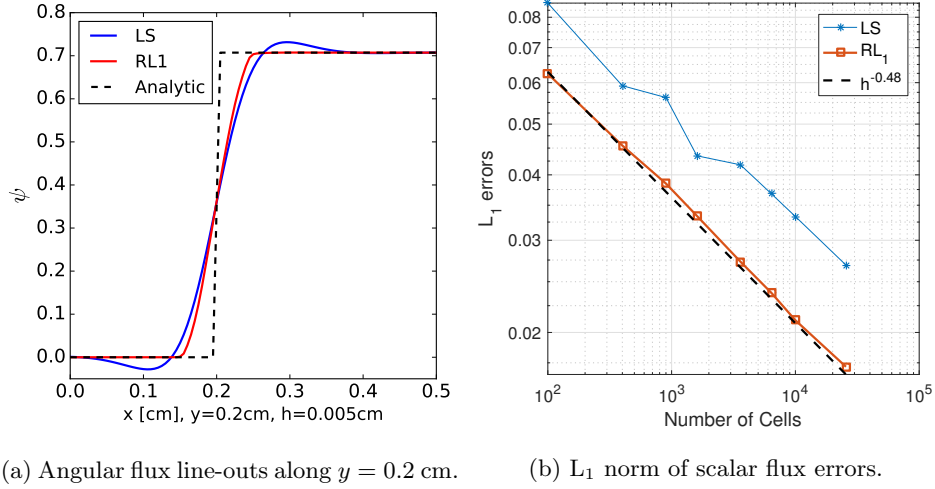


Figure 7: Angular flux line-out and scalar flux errors for the pure absorber test problem.

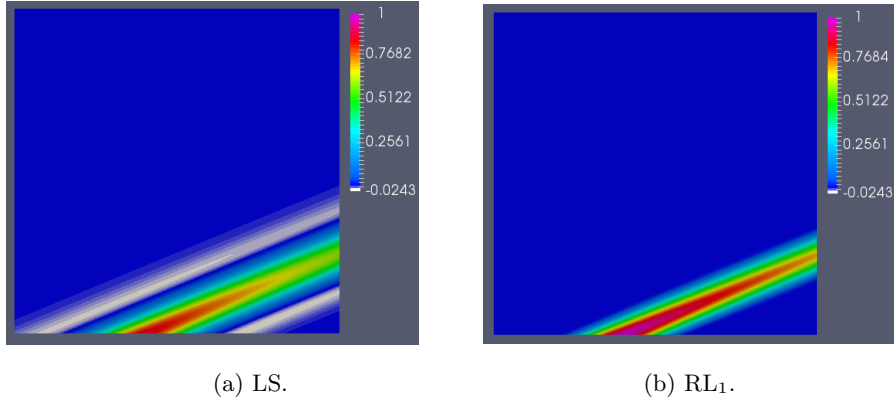


Figure 8: Angular flux distributions for the grazing incident.

Figure 8 illustrates the spatial distribution of angular flux for both methods. LS gives a negative angular flux even when the incident boundary condition is smooth in space. As the line-out plots presented in Figs. 9a (incident boundary) and 9b (outgoing boundary), with converged RL₁, we see agreement with the analytic solution except for slight smearing on the outgoing boundary in Figure 9b. Moreover, without convergence but with only one or two iterations

of residual weighting, RL_1 can still deliver acceptable results. On the other hand, LS solution presents negative solutions. Moreover, RL_1 , in contrast to IRLS[24, 25], treats the smooth incident data correctly and propagates the information correctly throughout the domain.

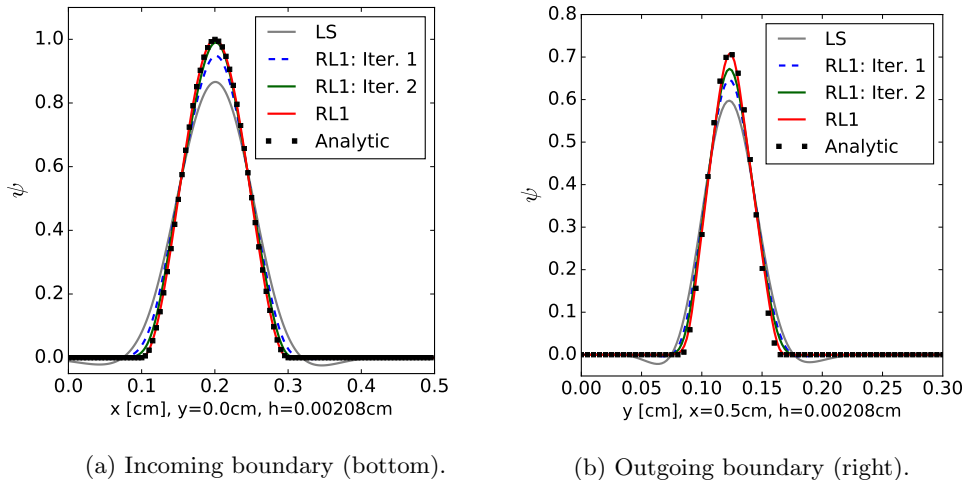
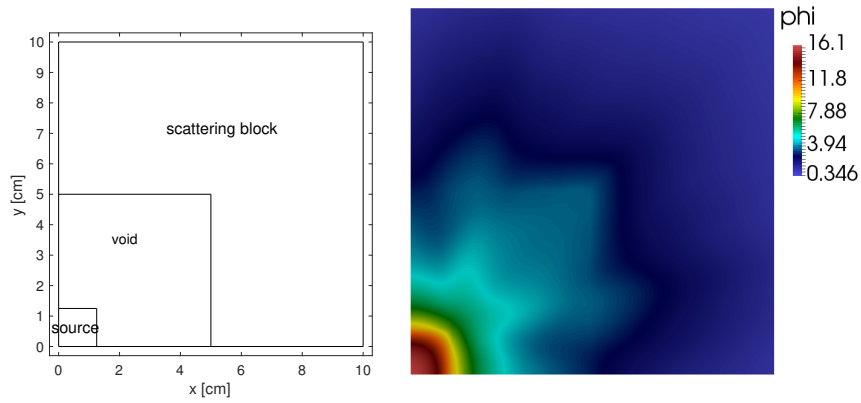


Figure 9: Boundary results comparison for smooth boundary problem.

4.4. Ackroyd test

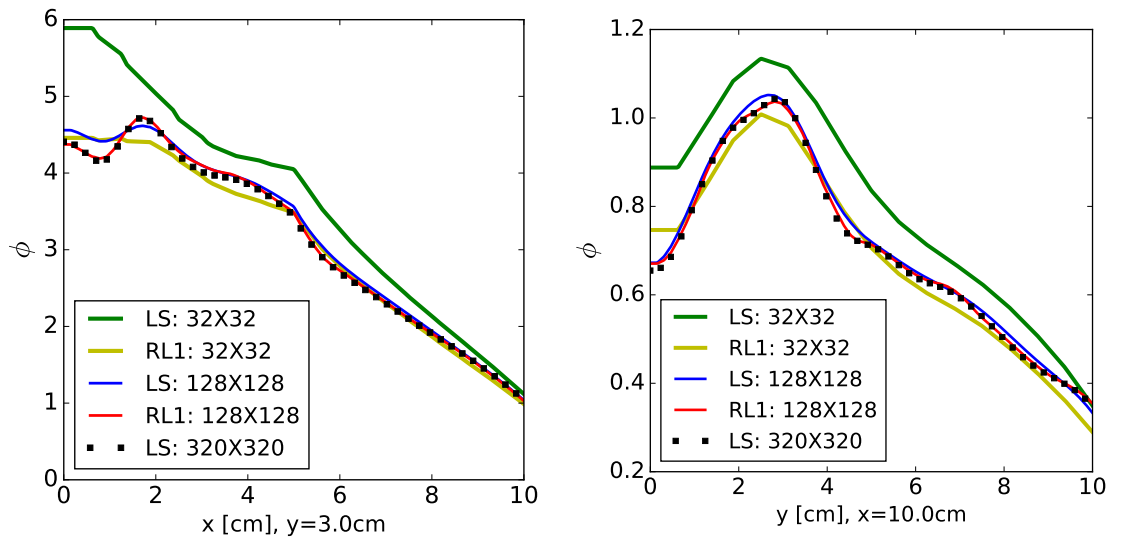
Finally, we present the results for the Ackroyd problem[32, 17]. This is a heterogeneous problem that has a high-scattering ratio central block and outer shield ($\sigma_t = 0.2, \sigma_s = 0.19$). There is a void between the block and the shield. See Fig. 10a for a schematic of a quarter of the problem geometry. The whole problem is symmetric about x-axis and y-axis. A reference scalar flux from an LS calculation using 320×320 cells with a Gauss-Chebyshev level-symmetric-like S_8 quadrature[33] is presented in Figure 10b. We examine the solution along a line that crosses the void in Figure 11a and another one on the boundary in Figure 11b. In both cases, the coarse mesh (32×32) RL_1 solution agrees reasonably well with the fine mesh LS results, while the LS coarse-mesh solution has large and noticeable errors. When refining to 128×128 , RL_1 agrees with the reference, while LS still has large errors.



(a) Ackroyd problem configuration.

(b) Ackroyd problem scalar flux distribution from LS solution with 320×320 cells and S_8 quadrature.

Figure 10: Ackroyd problem layout and reference solution.



(a) Solution across the void.

(b) Solution on right boundary.

Figure 11: Ackroyd problem line-out plots.

5. Concluding remarks and future work

In this work, we developed an effectively non-oscillatory regularized L_1 finite element scheme for solving radiation transport problems. Starting from minimizing the L_1 norm of transport residual, we derived a continuum form of L_1 finite element method along with a consistent nonlinear L_1 BC. The resulting continuum form is a weighted LS problem where the weight is the inverse of the absolute value of the residual. We regularize this form by switching the weight to unity when the residual is small. Numerical tests with void, pure absorber and heterogeneous problems demonstrate the efficacy and accuracy of our methodology.

There exist opportunities to improve our method. For one, our technique for solving the resulting nonlinear equations is based on fixed-point iteration. The universal efficiency of such a scheme is to be investigated. Other possibilities, such as Jacobian-free Newton Krylov method[34], could improve the efficiency of our scheme. Furthermore, our scheme inherits the properties of LS in that it is only conservative in the limit of the mesh size going to zero. Other authors have presented ways to ameliorate this issue (such as SAAF weighting for problems without void) and other void treatments [35, 36]. Another possibility is to use a high-order low-order formalism [37, 38] to solve the transport equation, where RL_1 is used for the high-order solve.

Acknowledgements

W. Zheng is thankful to Dr. Wolfgang Bangerth from Colorado State University for suggestions on the methodology derivation. Also, appreciation goes to Dr. Milan Hanus from Texas A&M University for fruitful discussions and helpful proofreading.

This project is funded by Department of Energy NEUP research grant from Battelle Energy Alliance, LLC- Idaho National Laboratory, Contract No: C12-00281.

References

References

- [1] E. W. Larsen, J. Morel, W. F. Miller, Asymptotic solutions of numerical transport problems in optically thick, diffusive regimes, *Journal of Computational Physics* 69 (2) (1987) 283–324.
- [2] E. W. Larsen, J. E. Morel, Asymptotic solutions of numerical transport problems in optically thick, diffusive regimes II, *Journal of Computational Physics* 83 (1) (1989) 212–236.
- [3] M. L. Adams, Discontinuous finite element transport solutions in thick diffusive problems, *Nuclear Science and Engineering* 137 (2001) 298–333.
- [4] R. G. McClarren, R. B. Lowrie, The effects of slope limiting on asymptotic-preserving numerical methods for hyperbolic conservation laws, *Journal of Computational Physics* 227 (23) (2008) 9711 – 9726.
- [5] V. M. Laboure, Improved fully-implicit spherical harmonics methods for first and second order forms of the transport equation using galerkin finite element, Ph.D. dissertation, Texas A&M University (2016).
- [6] W. Zheng, Least-squares and other residual based techniques for radiation transport calculations, PhD dissertation, Texas A&M University (2016).
- [7] W. F. Miller, E. E. Lewis, *Computational Methods of Neutron Transport*, 1st Edition, American Nuclear Society, 1993.
- [8] M. Hanuš, R. McClarren, On the use of symmetrized transport equation in goal-oriented adaptivity, *Journal of Computational and Theoretical Transport* (2016) 1–20.
- [9] J. E. Morel, J. M. McGhee, A Self-Adjoint Angular Flux Equation, *Nuclear Science and Engineering* 132 (3) (1999) 312–325.

- [10] Y. Wang, S. Schunert, M. DeHart, R. Matineau, W. Zheng, Hybrid P_N - S_N With Lagrange Multiplier and Upwinding for the Multiscale Transport Capability in Rattlesnake, Progress in Nuclear Energy (submitted on Sept. 2016).
- [11] W. Zheng, R. G. McClarren, Accurate Least-Squares PN Scaling based on Problem Optical Thickness for solving Neutron Transport Problems, Progress in Nuclear Energy (submitted on Sept. 2016).
- [12] V. M. Laboure, R. G. McClarren, Y. Wang, Globally Conservative, Hybrid Self-Adjoint Angular Flux and Least-Squares Method Compatible with Void, ArXiv e-prints [arXiv:1605.05388](https://arxiv.org/abs/1605.05388).
- [13] W. Zheng, R. G. McClarren, J. E. Morel, An Accurate Globally Conservative Subdomain Discontinuous Least-squares Scheme for Solving Neutron Transport Problems, ArXiv e-prints [arXiv:1612.01982](https://arxiv.org/abs/1612.01982).
- [14] J. Hansen, J. Peterson, J. Morel, J. E. Ragusa, Y. Wang, A Least-Squares Transport Equation Compatible with Voids, Journal of Computational and Theoretical Transport 43 (1-7) (2015) 374–401.
- [15] J. R. Peterson, H. R. Hammer, J. E. Morel, J. C. Ragusa, Y. Wang, Conservative Nonlinear Diffusion Acceleration Applied to the Unweighted Least-squares Transport Equation in MOOSE, in: M&C2015, 2015, nashville, TN, United States.
- [16] S. Schunert, Y. Wang, M. D. DeHart, R. C. Martineau, Hybrid P_N - S_N Calculations with SAAF for the Multiscale Transport Capability in Rattlesnake, in: PHYSOR 2016.
- [17] C. Drumm, Spherical harmonics (pn) methods in the sceptre radiation transport code, in: M&C 2015, 2015.
- [18] C. Ketelsen, T. Manteuffel, J. Schroder, Least-squares finite element discretization of the neutron transport equation in spherical geometry, SIAM Journal on Scientific Computing 37 (5) (2015) S71–S89.

- [19] W. Zheng, R. G. McClarren, Non-oscillatory Reweighted Least Square Finite Element Method for S_N Transport, in: ANS Winter Meeting 2015, Vol. 113, pp. 688–691.
- [20] W. Zheng, R. G. McClarren, Non-oscillatory Reweighted Least Square Finite Element for Solving P_N Transport, in: ANS Winter Meeting 2015, Vol. 113, pp. 692–695.
- [21] P. G. Maginot, J. E. Morel, J. C. Ragusa, A non-negative moment-preserving spatial discretization scheme for the linearized boltzmann transport equation in 1-d and 2-d cartesian geometries, *Journal of Computational Physics* 231 (20) (2012) 6801 – 6826.
- [22] P. Maginot, J. Morel, J. Ragusa, A positive non-linear closure for the sn equations with linear-discontinuous spatial differencing, 2009, m&C 2009, Saratoga Springs, New York, United States.
- [23] W. Zheng, R. G. McClarren, On Variable Selection and Effective Estimations of Interactive and Quadratic Sensitivity Coefficients: A Collection of Regularized Regression Techniques, in: M&C2015, 2015, nashville, TN, United States.
- [24] B. Jiang, Non-oscillatory and non-diffusive solution of convection problems by the iteratively reweighted least-square finite element method, *Journal of Computational Physics* 105 (1993) 108 – 121.
- [25] R. Lowrie, P. Roe, On the numerical solution of conservation laws by minimizing residuals, *Journal of Computational Physics* 113 (2) (1994) 304 – 308.
- [26] J. L. Guermond, A finite element technique for solving first order pdes in l_p , *SIAM J. Numer. Anal* 42 (2) (2004) 714–737.
- [27] R. E. Alcouffe, Diffusion Synthetic Acceleration Methods for Diamond-Differenced Discrete-Ordinates Equations, *Nuclear Science and Engineering* 64 (1977) 344–355.

- [28] C. L. Castrianni, M. L. Adams, A Nonlinear Corner-Balance Spatial Discretization for Transport on Arbitrary Grids, *Nuclear Science and Engineering* 128 (3) (1998) 278–296.
- [29] G. I. Bell, S. Glasstone, *Nuclear Reactor Theory*, 3rd Edition, Krieger Pub Co, Princeton, NJ, 1985.
- [30] R. Lin, Discontinuous Discretization for Least-Squares Formulation of Singularity Perturbed Reaction-Diffusion Problems in One and Two Dimensions, *SIAM J. NUMER. ANAL* 47 (1) (2008) 89–108.
- [31] W. Bangerth, D. Davydov, T. Heister, L. Heltai, G. Kanschat, M. Kronbichler, M. Maier, B. Turcksin, D. Wells, The `deal.II` library, version 8.4, *Journal of Numerical Mathematics* 24.
- [32] R. T. Ackroyd, J. G. Issa, N. S. Rivait, Treatment of Voids in Finite Element Transport Methods, *Prog. Nucl. Energy* 1 and 2 (1986) 85–89.
- [33] J. J. Jarrell, M. L. Adams, Discrete-ordinates quadrature sets based on linear discontinuous finite elements, 2011, m&C 2011, Rio de Janeiro, Brazil.
- [34] Jacobian-free Newton-Krylov methods: a survey of approaches and applications, *Journal of Computational Physics* 193 (2) (2004) 357 – 397.
- [35] V. M. Laboure, R. G. McClarren, Y. Wang, Globally conservative, hybrid self-adjoint angular flux and least-squares method compatible with void, arXiv preprint arXiv:1605.05388.
- [36] Y. Wang, H. Zhang, R. C. Martineau, Diffusion Acceleration Schemes for Self-Adjoint Angular Flux Formulation with a Void Treatment, *Nuclear Science and Engineering* 176 (2) (2014) 201–225.
- [37] S. R. Bolding, M. A. Cleveland, J. E. Morel, A high-order low-order algorithm with exponentially convergent monte carlo for thermal radiative transfer, *Nuclear Science and Engineering* 185 (1).

- [38] W. A. Wieselquist, D. Y. Anistratov, J. E. Morel, A cell-local finite difference discretization of the low-order quasidiffusion equations for neutral particle transport on unstructured quadrilateral meshes, *Journal of Computational Physics* 273 (2014) 343–357.